Journal of Power Sources 251 (2014) 237–242

Contents lists available at ScienceDirect

Journal of Power Sources

journal homepage: www.elsevier.com/locate/jpowsour

Growth of single-crystalline β-$Na_{0.33}V_2O_5$ nanowires on conducting substrate: A binder-free electrode for energy storage devices

Nguyen Thi Hong Trang, Niranjanmurthi Lingappan, Imran Shakir, Dae Joon Kang*

Department of Physics, Department of Energy Science, Institute of Basic Sciences, and SKKU Advanced Institute of Nanotechnology, Sungkyunkwan University, Suwon 440-746, Republic of Korea

HIGHLIGHTS

- Single-crystalline β-$Na_{0.33}V_2O_5$ nanowires grown on a Pt-coated silicon substrate.
- Nanowires with the diameter of ~150 nm and a length over 5 μm formed.
- The as-grown nanowires used as a binder free electrode for supercapacitors.
- The enhanced electrochemical performances due to the rationally designed electrode.

GRAPHICAL ABSTRACT

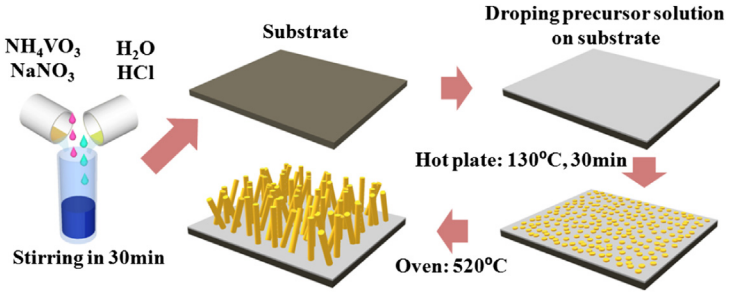

ARTICLE INFO

Article history:
Received 20 September 2013
Received in revised form
14 November 2013
Accepted 16 November 2013
Available online 23 November 2013

Keywords:
Beta sodium vanadate nanowires
Chemical solution deposition
Intercalation pseudocapacitance
Supercapacitors

ABSTRACT

We demonstrate the catalyst-free growth of single-crystalline β-$Na_{0.33}V_2O_5$ nanowires on a Pt-coated silicon substrate ($Pt/SiO_2/Si$) using a chemical solution deposition method, the result of which is then used as a binder-free electrode for high-performance energy storage devices. Scanning electron micrograph indicates that nanowires with a uniform diameter of ~150 nm and a length greater than 5 μm are formed. When evaluated as an electrode for supercapacitors, the crystalline β-$Na_{0.33}V_2O_5$ nanowires are found to have favorable characteristics, including a specific capacitance of 498 F g^{-1} at a current density of 0.4 A g^{-1}, and a moderate rate capability with a Coulombic efficiency of 96% after 1500 cycles. In addition, the electrode shows a high energy density of 99.6 W h kg^{-1} at a power density of 485 W kg^{-1}. Such superior capacitive performance may be attributed to the high electrical conductivity and redox pseudocapacitance, as well as intercalation pseudocapacitance, arising from the layered structure of the materials and the high crystallinity of nanowires. This outstanding electrochemical performance will make β-$Na_{0.33}V_2O_5$ nanowires a promising electrode material for high-performance supercapacitors.

1. Introduction

High fuel prices and the global warming crisis have stimulated intense research into energy storage devices for a wide range of applications, including hybrid electric vehicles, smart grid, and portable electronics [1–3]. In this regard, supercapacitors have been considered an attractive choice for next-generation energy storage systems, owing to their high power density, long-term cycling stability, and rapid charge/discharge processes [4,5]. Despite significant research, the energy density of supercapacitors is still far from meeting the requirements of the aforementioned applications. Thus, the development of electrode materials with high energy density is one of the hottest topics in current energy storage research. Among various electrode materials, transition metal oxides have been considered as a potential candidate owing to their high theoretical specific capacitance.

* Corresponding author. Tel.: +82 31 290 5906; fax: +82 31 290 5947.
E-mail address: djkang@skku.edu (D.J. Kang).

0378-7753/$ – see front matter © 2013 Elsevier B.V. All rights reserved.
http://dx.doi.org/10.1016/j.jpowsour.2013.11.041

Recently, transition metal oxides with layered structures have emerged as a new branch of electrode materials for supercapacitors because of their unique charge storage mechanism [6,7]. A high specific capacitance can be achieved from such systems via the application of one of two principles, redox pseudocapacitance, or intercalation pseudocapacitance. The former concerns the electrochemical adsorption of ions onto the surface of the electroactive materials, while the latter arises from the electrochemical adsorption of ions in the gap between the interlayer spacing of layered-structures materials. Various metal oxides with a layer structure have been investigated for their ability to intercalate ions in a wide range of sites, such as MnO_2 [8], RuO_2 [9], NiO [10], V_2O_5 [11]. Most metal oxides, however, including the aforementioned, suffer from poor electrical conductivity, which limits overall performance. Developing materials with larger interlayer separation and higher electrical conductivity is therefore of great importance.

The beta phase of sodium vanadate (β-$Na_{0.33}V_2O_5$) is one of the most appealing candidates owing to its unique structural arrangements and high electrical conductivity [12,13]. β-$Na_{0.33}V_2O_5$ has the larger interlayer spacing and tunnel-like structure along the *b* axis, with three types of vanadium sites (V_1, V_2 and V_3), which is expected to enhance the ion intercalation within this structure. In addition, the tunnel structure can act as a conducting channel for fast ion diffusion, which can significantly improve the overall charge storage kinetics.

More recently, the binder-free electrode systems have been actively investigated as high performance electrodes for energy storage devices, due to their enhanced electrochemical performances as compared with the conventional electrode systems. In this approach, the electrode materials are directly grown on the current collectors avoiding the use of other auxiliary materials such as conductive agents and binders [14,15].

In this study, we demonstrate a facile method to grow single-crystalline β-$Na_{0.33}V_2O_5$ nanowires directly onto a Platinum-coated silicon ($Pt/SiO_2/Si$) substrate using a solution deposition method without any additional catalyst. The defect-free nanowires on the conducting substrate can be used as a binder-free electrode for energy storage devices. When evaluated as electrode supercapacitors, the nanowires exhibit a high specific capacitance of 498 F g^{-1} at a current density of 0.4 A g^{-1}, excellent rate capability, and an average Coulombic efficiency of 96.5% after 1500 cycles. Based on their outstanding electrochemical performance, β-$Na_{0.33}V_2O_5$ nanowires are a promising candidate for future energy storage device work.

2. Experimental

2.1. Synthesis of β-$Na_{0.33}V_2O_5$ nanowires on the $Pt/SiO_2/Si$ substrate

Ammonium metavanadate (NH_4VO_3), and sodium nitrate ($NaNO_3$) (Sigma Aldrich, South Korea) were used as precursors. The precursor solution was deposited on the $Pt/SiO_2/Si$ substrates using a spin coating technique. Before dropping solution, the substrates were cleaned via immersion in a progression of acetone, ethanol, and DI water, and then dried with nitrogen. 0.1 mmol of NH_4VO_3 and 0.02 mmol of $NaNO_3$ were dissolved in 5 mL of DI water to obtain the precursor solution. The pH of the solution was adjusted to 2 using HCl, and stirred at ambient temperature for 30 min. Typically, 1 mL of the aforementioned solution was drop-casted on 1 × 1 cm^2 $Pt/SiO_2/Si$ substrate and heated on a hot plate at 130 °C for 30 min, and then annealed at 520 °C for 4 h to obtain single-crystalline β-$Na_{0.33}V_2O_5$ nanowires. The typical mass of the nanowires was estimated to be 0.8 mg cm^{-2}.

2.2. Characterization

The pyrolysis of the sodium vanadate precursor was investigated via thermo-gravimetric (TGA) (Seiko Exstar 6000 TGA/DT 6100) analysis in an air atmosphere with a linear temperature ramp of 5 °C min^{-1} over the temperature range of 25 °C–600 °C. The crystal structure of the β-$Na_{0.33}V_2O_5$ nanowires grown on the $Pt/SiO_2/Si$ substrate was studied via X-ray diffraction (XRD) (D8 FOCUS 2200 V, Bruker AXS), using Cu Kα radiation ($\lambda = 1.5418$ Å). The morphology of the nanowires was examined via field emission scanning electron microscopy (FE-SEM) (JEOL JSM-7401F) and high-resolution transmission electron microscopy (HRTEM) (FE-TEM JEM2100F) operated with an accelerating voltage of 300 kV. The composition and the oxidation states of the nanowires were determined using X-ray photoelectron spectroscopy (XPS) (ESCALAB spectrometer, VG Scientific), with a monochromic Mg K_α light source.

2.3. Electrochemical measurements

The electrochemical measurements were carried out in a conventional, three-electrode cell with a CHI-660B electrochemical station (CH Instruments Inc., TX, USA), using 1 M $LiClO_4$/propylene carbonate as the electrolyte. As-grown β-$Na_{0.33}V_2O_5$ nanowires on the $Pt/Si/SiO_2$ substrate were used as a working electrode, without the addition of a conductive agent or polymeric binder. The platinum wire and a saturated calomel electrode were used as the counter and reference electrodes, respectively.

3. Results and discussion

Scheme 1 illustrates the synthesis of single-crystalline β-$Na_{0.33}V_2O_5$ nanowires onto a $Pt/SiO_2/Si$ substrate. The TGA-DTG curves (Fig. 1(a)) of the precursor show a two-step decomposition profile. The initial weight loss below 150 °C is due primarily to the evaporation of water molecules, while the major weight loss occurred in the temperature range of 150 °C–480 °C. This can be attributed to the decomposition of the NH_4VO_3 and $NaNO_3$. This typical decomposition profile is further utilized as a reference pattern to elucidate the formation mechanism of β-$Na_{0.33}V_2O_5$ nanowires. The growth mechanism is proposed based on Refs. [16–18].

At temperature higher than 200 °C, as can be seen from TGA result (Fig. 1(a)), the weight loss becomes significant and thus the NH_4VO_3 is expected to be decomposed as follows [16]

$$NH_4VO_3 + HCl \rightarrow NH_4Cl + HVO_3$$

$$HVO_3 \rightarrow V_2O_5 + H_2O$$

Thus, we have the follow reaction

$$2NH_4VO_3 + 2HCl = 2NH_4Cl + V_2O_5 + H_2O \quad (1)$$

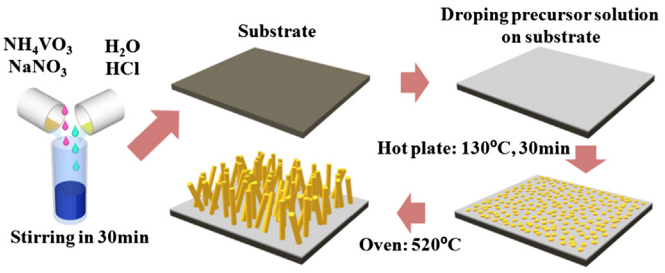

Scheme 1. Schematic illustration of the growth of β-$Na_{0.33}V_2O_5$ nanowires directly on $Pt/SiO_2/Si$ substrate via chemical solution deposition method.

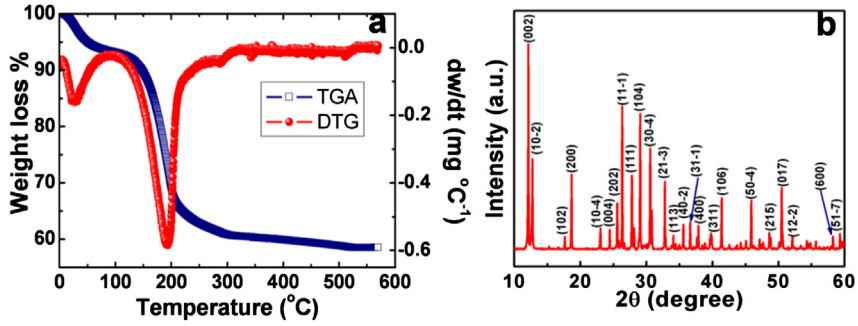

Fig. 1. (a) Thermo-gravimetric analysis curve of the β-$Na_{0.33}V_2O_5$ precursor in an air atmosphere with a linear temperature ramp of 5 °C min^{-1} over the temperature range of 25 °C–600 °C (b) XRD pattern of β-$Na_{0.33}V_2O_5$ nanowires grown at 520 °C for 4 h.

In this reaction, the NO_3^- ions can enhance the reaction of V_2O_5 by nucleophilic substitution [17]

$$V_2O_5 + Cl^- \rightarrow VO_3^- + VO_2Cl$$

$$VO_2Cl + H_2O \rightarrow VO_3^- + Cl^- + 2H^+$$

$$2NaNO_3 + V_2O_5 + H_2O = 2NaVO_3 + 2HNO_3, \quad (2)$$

It should be pointed out that Cl^- ions can enhance the dissolution and plays as reducing agent to convert partly vanadium oxide V^{5+} (in V_2O_5 form) to V^{4+} (in β-$Na_{0.33}V_2O_5$ form) [18]

$$6NaVO_3 + 4HCl = NaV_6O_{15}\ (\beta\text{-}Na_{0.33}V_2O_5) + 2H_2O + 4NaCl \quad (3)$$

The crystalline nature of the as-grown nanowires was investigated via XRD, as shown in Fig. 1(b). All of the diffraction peaks can be perfectly assigned to the JCPDS file (86-0120) of the monoclinic phase of β-$Na_{0.33}V_2O_5$; however, no obvious diffraction peaks from other phases are observed, indicating the high quality of the nanowires.

The morphology of the β-$Na_{0.33}V_2O_5$ nanowires was examined using FESEM as shown in Fig. 2. The low-magnification FESEM image clearly indicates that the high-density nanowires are uniformly grown on the entire substrate. The high-magnification (Fig. 2(b)) and cross-section (Fig. 2(c)) FESEM images reveal that the typical diameter of the nanowires is ~150 nm, with a length of ~5 μm.

To further investigate the crystal structure and growth direction of the β-$Na_{0.33}V_2O_5$ nanowires in detail, HRTEM and selected area diffraction (SAED) patterns were performed. As depicted in Fig. 3(a), the HRTEM image shows an individual β-$Na_{0.33}V_2O_5$ nanowire with a diameter of 150 nm. Fig. 3(b) indicates highly single crystalline atomic arrangements in which the lattice fringes are clearly visible. The distance between the neighboring fringes is approximately 2.39 Å, which corresponds to the (006) lattice plane of monoclinic β-$Na_{0.33}V_2O_5$. Furthermore, the SAED pattern as shown in Fig. 3(c), which unveils the single crystalline nanowires with a preferential growth direction along the <001> direction, which agrees with the XRD result.

The chemical state of the as-grown β-$Na_{0.33}V_2O_5$ nanowires was analyzed via XPS measurement. As can be seen in Fig. 4(a), the high resolution XPS spectrum of V2p can be deconvoluted into four peaks at 515.6, 517.2, 523.7 and 525.1 eV correspond to V^{4+}2p3/2, V^{5+} 2p3/2, V^{4+}2p1/2 and V^{5+}2p1/2, respectively [19]. In addition, the appearance of two peaks at 518.9 and 521.1 eV is attributed to the X-ray satellite of the O1s core level [20]. The oxidation states of vanadium (+5 and +4) are in good agreement with previous reports [12]. Such overlapping peaks are usually observed in ternary vanadium oxide bronzes containing mixed valences of V^{5+} and V^{4+} [13–15]. The area under the curve reflects the actual population of the respective species, thus allowing the relative areas for the V^{5+} and V^{4+} states to be computed. The core-level O1s spectrum of nanowires (Fig. 4(b)) can be further deconvoluted into the three peaks at 529.9, 530.7 and 533.0 eV. The BE presented by the first peak (529.9 eV) can be associated to the V–O bonding in the V_2O_5 [19,21]. The second peak (530.7 eV) and the third peak (533.0 eV) can be assigned to chemisorbed OH and ambient C=O [22]. The Na1s spectra (two peaks at 1071.2 eV and 1072.3 eV) confirm the presence of Na atoms occupying the lattice positions along the *b* axis of β-$Na_{0.33}V_2O_5$, as shown in Fig. 4(c), [19].

The high-quality, single-crystalline β-$Na_{0.33}V_2O_5$ nanowires on Pt/SiO_2/Si substrate can be used as a binder-free electrode for various energy storage devices. For instance, the as-grown β-$Na_{0.33}V_2O_5$ nanowires are used as an electrode for supercapacitors. The electrochemical properties of nanowires were investigated via cyclic voltammetry (CV) and galvanostatic charge/discharge techniques. Fig. 5(a) shows the CV of the β-$Na_{0.33}V_2O_5$ nanowires at a scan rate of 5 mV s^{-1}, with the electrolyte of 1 M $LiClO_4$/PC. The shape of the curve clearly reveals pseudocapacitive characteristics. Two-pairs of well-resolved redox peaks at +0.12 V/+0.38 V and −0.11 V/−0.25 V are observed within a wide-potential range

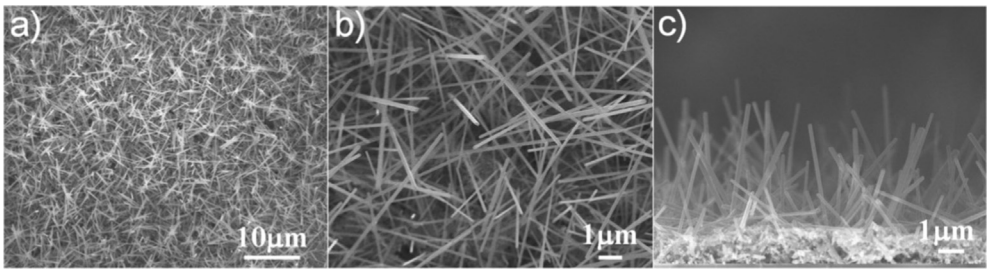

Fig. 2. Low magnification (a), high magnification (b) and cross-section (c) FE-SEM images of as-grown β-$Na_{0.33}V_2O_5$ nanowires.

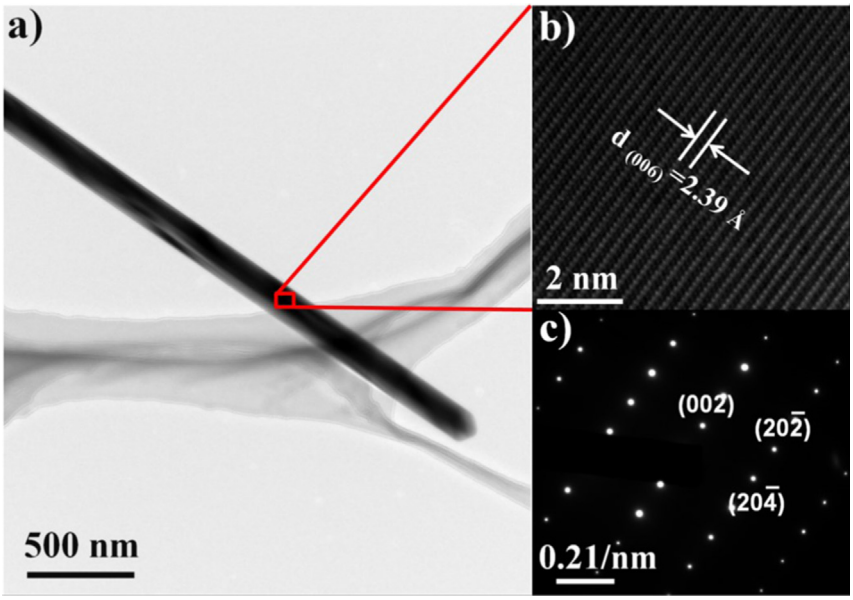

Fig. 3. (a) Low magnification TEM image of individual β-$Na_{0.33}V_2O_5$ nanowire. (b) HR-TEM of nanowire showing high crystallinity. (c) SAED pattern of an individual nanowire shows the growth direction of nanowire along the *c* axis.

of −0.6 to 0.6 V. The typical redox peaks arise from Li insertion/deinsertion of β-$Na_{0.33}V_2O_5$ nanowires, according to the following electrochemical reaction [23]

$$Na_{0.33}V_2O_5 + xe^- + xLi^+ \leftrightarrow 4Li_xNa_{0.33}V_2O_5 \quad (4)$$

where *x* represents the Li intercalation level.

The CV curves of the β-$Na_{0.33}V_2O_5$ nanowires with various scan rates, ranging from 1 to 100 mV s^{-1}. As can be seen in Fig. 5(b), the shape of the CV curves show almost no change with the increase in the scan rate, implying the improved mass transportation, excellent electron conduction within the structure, and small equivalent series resistance. With the increase in scan rates, only a small shift in peak position was observed, which in turn, indicates the internal resistance of the electrode should be small [24,25].

Obviously, the main resistance in this system arises from the organic electrolyte, which possesses moderate ionic and electrical conductivities as compared to aqueous based electrolyte. However, with its extended voltage windows due to organic electrolyte, we can obtain high energy density as can be seen in recent report [26].

The variation in specific capacitance of the β-$Na_{0.33}V_2O_5$ nanowires as a function of scan rate is plotted in Fig. 5(c). A high specific capacitance of 620 F g^{-1} can be obtained at 1 mV s^{-1}, which is significantly higher than a single component system such as MoV_2O_8 [20], MnO_2 [27], NiO [28], V_2O_5 [29]. This high specific capacitance results from both redox pseudocapacitance and Li intercalation pseudocapacitance of the layered structure. As expected, the specific capacitance decreases as the scan rate increases. When the scan rate increased to 50 mV s^{-1}, the nanowire electrode still exhibits 148 F g^{-1}, and maintained approximately 30% of its initial capacitance. This phenomenon is most likely due to the limited accessibility of the electrolyte ions to the surface of the active materials.

We believe that the total charge stored within this material consist of two components: Li ion intercalation and charge-transfer at the oxide–electrolyte interface. Due to the kinetic limitation in the interfacial charge transfer process, the surface-dependent capacitance dominates the overall capacitance at higher scan rates [30]. In contrast; the intercalation capacitance contributes the major portion of the overall capacitance at slow scan rates and decreases with the increase in scan rate. These observations agree well with the charge storage mechanisms, as: (1) the surface reaction has a capacitive response with fast reaction kinetics, hence it dominates at fast scan rate, and (2) the diffusion-controlled intercalation process is a slow reaction. It dominates at slow scan rates because longer times are required for effective ion intercalation.

Rate capability is one of the important measurements used to calculate the power and energy densities of β-$Na_{0.33}V_2O_5$ nanowires. The galvanostatic charge/discharge curves of the nanowires at different current densities are shown in Fig. 5(d). The symmetric

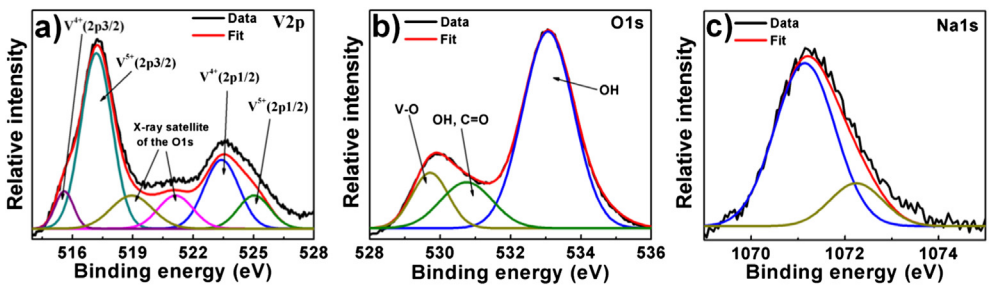

Fig. 4. High-resolution XPS spectra of (a) vanadium V 2p (b) oxygen O 1s and (c) sodium Na 1s regions of β-$Na_{0.33}V_2O_5$ nanowires.

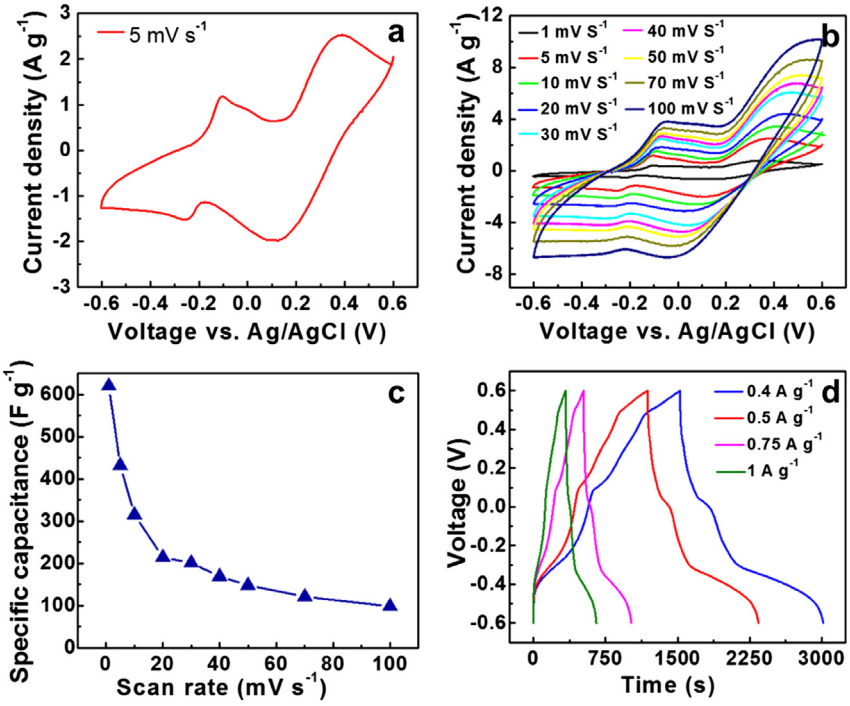

Fig. 5. (a) Cyclic voltammogram (CV) of β-$Na_{0.33}V_2O_5$ nanowires at the scan rate of 5 mV s^{-1}, (b) CV of β-$Na_{0.33}V_2O_5$ nanowires at different scan rates, (c) Specific capacitance variation of the nanowires as a function of the cycle number at 20 mV s^{-1} and (d) Charge/discharge curves of β-$Na_{0.33}V_2O_5$ nanowires at different current densities.

nature of the curve indicates the superior electrochemical characteristics, rapid reversible redox reaction and high electrical conductivity of the binder-free electrode. Furthermore, the specific capacitance is plotted in Fig. 6(a) as a function of current densities. It is worth noting that the specific capacitance is as high as 498, 481, 311 and 267 F g^{-1} for the discharge current densities of 0.4, 0.5, 0.75 and 1.0 A g^{-1}, respectively. This high rate capability of the β-$Na_{0.33}V_2O_5$ nanowires can be attributed to the high electrical conductivity of the nanowires directly grown on the conducting substrate.

The relationship between electrochemical performance and electrode kinetics was further investigated using electrochemical

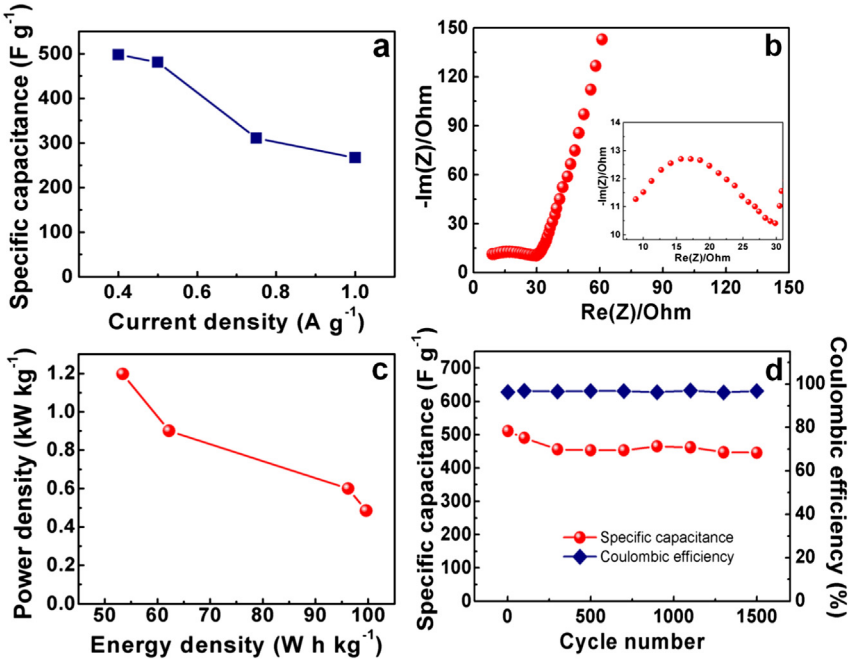

Fig. 6. (a) Variation of specific capacitance at different current densities, (b) Nyquist plot of the β-$Na_{0.33}V_2O_5$ nanowires in the frequency range from 0.01 Hz to 100 kHz, (c) Ragone chart of the supercapacitor obtained from the discharge curves measured at different current densities and (d) Cycling stability and Coulombic efficiency of the as-grown β-$Na_{0.33}V_2O_5$ nanowire based electrode.

impedance spectroscopy in the range of 100 kHz to 0.01 Hz. Fig. 6(b) shows the Nyquist plot of the β-$Na_{0.33}V_2O_5$ nanowires. It can be seen that the β-$Na_{0.33}V_2O_5$ nanowires exhibit a depressed semicircle in the high-middle frequency region, and a straight line in the low frequency range. The small diameter of the semicircle clearly indicates that the electrode possesses low contact and charge-transfer impedances, resulting in a significant improvement in the rate performance.

Power and energy densities are the two critical parameters used for evaluating electrochemical performance of supercapacitors. Fig. 6(c) shows the Ragone plot of the β-$Na_{0.33}V_2O_5$ nanowires. Single-crystalline β-$Na_{0.33}V_2O_5$ nanowires exhibit an ultrahigh energy density of 99.6 W h kg^{-1} at the power density of 485 W kg^{-1}, and the highest power density of 1200 W kg^{-1} at 53 W h kg^{-1}. This energy density is substantially higher than the values reported for V_2O_5-based electrodes, such as V_2O_5/CNT composite [31], V_2O_5 nanoribbons [32], and β-$Na_{0.33}V_2O_5$ nanobelt systems [16]. Such high energy density can be obtained primarily due to the high specific capacitance and large voltage window (1.2 V) of the β-$Na_{0.33}V_2O_5$ nanowires. The Table S1 in the Supporting information provides comparisons between our results and other vanadium oxide-based supercapacitors [20,31,33–35].

The long-term cycling stability of the β-$Na_{0.33}V_2O_5$ nanowires was measured at a scan rate of 10 mV s^{-1} for 1500 cycles. As shown in Fig. 5(d), the binder-free electrode exhibits excellent capacity retention of 90%, with a Coulombic efficiency of over 96%, even after 1500 cycles. This high cycling stability results from the high mechanical stability of the electrode, which is in turn due to the strong interfacial adhesion between the nanowires and current collector, which retained its mechanical stability during the charge/discharge processes.

Thus, the superior performance of the β-$Na_{0.33}V_2O_5$ nanowires can be attributed to the unique structural features of the single crystalline nanowires. First, the high electrical conductivity of the nanowires facilitates the fast ion and electron transport. Second, the high specific capacitance is obtained from the both faradaic capacitance and intercalation capacitance, which leads to the high energy density of the electrode. Third, the Pt/SiO_2/Si substrate enhances the conductivity of the overall electrode, and facilitates the charge transport due to the good adhesion between the electroactive material and the substrate. Furthermore, the high mechanical stability of the substrate maintains the structural integrity of the electrode during the repeated charge/discharge processes.

4. Conclusion

We have demonstrated a facile chemical deposition method for growing high-quality, single-crystalline β-$Na_{0.33}V_2O_5$ nanowires on the Pt/SiO_2/Si substrates without the need for an additional catalyst. The as-grown nanowires are used as a binder-free electrode for energy storage devices. As a proof-of-concept, the β-$Na_{0.33}V_2O_5$ nanowires are tested, and exhibits an excellent specific capacitance of 498 F g^{-1} at a current density of 0.4 A g^{-1}, and an excellent rate capability with a cycling efficiency of 90% after 1500 cycles. The superior performance of the nanowires is primarily attributed to the redox pseudocapacitance and intercalation pseudocapacitance resulting from the layered structure, high electrical conductivity, and good adhesion between the nanowires and the current collector. The effective cost, environmental friendly nature, and high capacitive performance make this material a promising candidate for practical advances in energy storage.

Acknowledgments

This research was supported by Basic Science Research Program through the National Research Foundation of Korea (NRF) funded by the Ministry of Education (2012R1A6A1040282).

Appendix A. Supplementary data

Supplementary data related to this article can be found at http://dx.doi.org/10.1016/j.jpowsour.2013.11.041

References

[1] M. Armand, J.M. Tarascon, Nature 451 (2008) 652–657.
[2] J.M. Tarascon, M. Armand, Nature 414 (2001) 359–367.
[3] J.S. Lee, S. Tai Kim, R. Cao, N.S. Choi, M. Liu, K.T. Lee, J. Cho, Adv. Energy Mater. 1 (2011) 34–50.
[4] P. Simon, Y. Gogotsi, Nat. Mater. 7 (2008) 845–854;
G. Wang, L. Zhang, J. Zhang, Chem. Soc. Rev. 41 (2012) 797–828.
[5] M.D. Stoller, S. Park, Z. Yanwu, J. An, R.S. Ruoff, Nano Lett. 8 (2008) 3498–3502.
[6] T. Brezesinski, J. Wang, S.H. Tolbert, B. Dunn, Nat. Mater. 9 (2010) 146–151.
[7] V. Augustyn, J. Come, M.A. Lowe, J.W. Kim, P.-L. Taberna, S.H. Tolbert, H.D. Abruña, P. Simon, B. Dunn, Nat. Mater. 12 (2013) 518–522.
[8] M. Toupin, T. Brousse, D. Bélanger, Chem. Mater. 16 (2004) 3184–3190.
[9] J.P. Zheng, P.J. Cygan, T.R. Jow, J. Electrochem. Soc. 142 (1995) 2699–2703.
[10] B. Wang, J.S. Chen, Z. Wang, S. Madhavi, X.W. Lou, Adv. Energy Mater. 2 (2012) 1188–1192.
[11] H.Y. Lee, J.B. Goodenough, J. Solid State Chem. 148 (1999) 81–84.
[12] H. Yamada, Y. Ueda, J. Phys. Soc. Jpn. 68 (1999) 2735–2740.
[13] S. Iwanaga, M. Marciniak, R.B. Darling, F.S. Ohuchi, J. Appl. Phys. 101 (2007), 123709.
[14] J. Jiang, Y. Li, J. Liu, X. Huang, C. Yuan, X.W. Lou, Adv. Mater. 24 (2012) 5166–5180.
[15] G.Q. Zhang, H.B. Wu, H.E. Hoster, M.B. Chan-Park, X.W. Lou, Energy Environ. Sci. 5 (2012) 9453–9456.
[16] E. Khoo, J. Wang, J. Ma, P.S. Lee, J. Mater. Chem. 20 (2010) 8368–8374.
[17] J.C. Yu, Yu Ho, Jiang Zhang, Chem. Mater. 14 (2002) 3808–3816.
[18] J. Yu, J.C. Yu, W. Ho, L. Wu, X. Wang, J. Am. Chem. Soc. 126 (2004) 3422–3423.
[19] V. Bondarenka, A. Martunas, S. Kaiciulis, L. Pandolfi, J. Electron Spectrosc. Relat. Phenom. 131–132 (2003) 99–103.
[20] M. Shahid, J. Liu, Z. Ali, I. Shakir, M.F. Warsi, J. Power Sources 230 (2013) 277–281.
[21] G. Silversmit, D. Depla, H. Poelman, G.B. Marin, R. De Gryse, Surf. Sci. 600 (2006) 3512–3517.
[22] J.C. Yu, W. Ho, J. Yu, S.K. Hark, K. Iu, Langmuir 19 (2003) 3889–3896.
[23] H. Liu, Y. Wang, L. Li, K. Wang, E. Hosono, H. Zhou, J. Mater. Chem. 19 (2009) 7885–7891.
[24] J. Yan, Z. Fan, W. Sun, G. Ning, T. Wei, Q. Zhang, R. Zhang, L. Zhi, F. Wei, Adv. Energy Mater. 22 (2012) 2632–2641.
[25] Y. Liang, F. Liang, H. Zhong, Z. Li, R. Fu, D. Wu, J. Mater. Chem. A 1 (2013) 7000–7005.
[26] L. Jiang, R. Zou, W. Li, J. Sun, X. Hu, Y. Xue, G. He, J. Hu, J. Mater. Chem. A 1 (2013) 478–481.
[27] M. Ghaemi, F. Ataherian, A. Zolfaghari, S.M. Jafari, Electrochim. Acta 53 (2008) 4607–4614.
[28] U.M. Patil, R.R. Salunkhe, K.V. Gurav, C.D. Lokhande, Appl. Surf. Sci. 255 (2008) 2603–2607.
[29] G. Wee, H.Z. Soh, Y.L. Cheah, S.G. Mhaisalkar, M. Srinivasan, J. Mater. Chem. 20 (2010) 6720–6725.
[30] B.E. Conway, V. Birss, J. Wojtowicz, J. Power Sources 66 (1997) 1–14.
[31] Z. Chen, Y. Qin, D. Weng, Q. Xiao, Y. Peng, X. Wang, H. Li, F. Wei, Y. Lu, Adv. Energy Mater. 19 (2009) 3420–3426.
[32] Q.T. Qu, Y. Shi, L.L. Li, W.L. Guo, Y.P. Wu, H.P. Zhang, S.Y. Guan, R. Holze, Electrochem. Commun. 11 (2009) 1325–1328.
[33] Z. Chen, V. Augustyn, J. Wen, Y. Zhang, M. Shen, B. Dunn, Y. Lu, Adv. Mater. 23 (2011) 791–795.
[34] A. Ghosh, E.J. Ra, M. Jin, H.-K. Jeong, T.H. Kim, C. Biswas, Y.H. Lee, Adv. Energy Mater. 21 (2011) 2541–2547.
[35] R.N. Reddy, R.G. Reddy, J. Power Sources 156 (2006) 700–704.